UNIVERSITÉ DE GENÈVE

Archive ouverte UNIGE
https://archive-ouverte.unige.ch

Article scientifique | Article | 2022

Published version | Open Access

This is the published version of the publication, made available in accordance with the publisher's policy.

Effect of excitation wavelength (blue vs near UV) and dopant concentrations on afterglow and fast decay of persistent phosphor $SrAl_2O_4:Eu^{2+},Dy^{3+}$

Walfort, Bernhard; Gartmann, Nando; Afshani Aghajari, Jafar; Rosspeintner, Arnulf; Hagemann, Hans-Rudolf

How to cite

WALFORT, Bernhard et al. Effect of excitation wavelength (blue vs near UV) and dopant concentrations on afterglow and fast decay of persistent phosphor $SrAl_2O_4:Eu^{2+},Dy^{3+}$. In: Journal of Rare Earths, 2022, vol. 40, n° 7, p. 1022–1028. doi: 10.1016/j.jre.2021.07.014

This publication URL: https://archive-ouverte.unige.ch/unige:181758

Publication DOI: 10.1016/j.jre.2021.07.014

© The author(s). This work is licensed under a Creative Commons Attribution-NonCommercial-NoDerivatives (CC BY-NC-ND 4.0) https://creativecommons.org/licenses/by-nc-nd/4.0

Journal of Rare Earths 40 (2022) 1022–1028

Contents lists available at ScienceDirect

Journal of Rare Earths

journal homepage: http://www.journals.elsevier.com/journal-of-rare-earths

Effect of excitation wavelength (blue vs near UV) and dopant concentrations on afterglow and fast decay of persistent phosphor $SrAl_2O_4:Eu^{2+},Dy^{3+}$☆

Bernhard Walfort [a], Nando Gartmann [a], Jafar Afshani [b], Arnulf Rosspeintner [b], Hans Hagemann [b,*]

[a] LumiNova AG, Switzerland, Speicherstrasse 60a, CH-9053, Teufen, Switzerland
[b] Dépt. de Chimie Physique, Université de Genève, 30, Quai E. Ansermet, CH 1211, Geneva 4, Switzerland

ARTICLE INFO

Article history:
Received 5 March 2021
Received in revised form
14 July 2021
Accepted 26 July 2021
Available online 28 July 2021

Keywords:
Persistent phosphor
Strontium aluminate
Europium
Förster energy transfer
Rare earths

ABSTRACT

The persistent phosphor $SrAl_2O_4:Eu^{2+},Dy^{3+}$ is the subject of numerous investigations. One often neglected aspect is that in this phosphor, as well as in $Sr_4Al_{14}O_{25}:Eu^{2+},Dy^{3+}$, there are two different Sr^{2+} sites which can be occupied by the dopant Eu^{2+} ions. We first introduce a general scheme of possible energy transfers in these persistent phosphor materials including explicitly both europium ions. This scheme is used as a generic starting point to study experimentally specific pathways. We illustrate this application with the study of the effect of excitation wavelength (444 and 382 nm) on the afterglow of differently doped $SrAl_2O_4:Eu^{2+},Dy^{3+}$ samples, as well as on the emission decay curves. With the same excitation intensity under 444 nm excitation, the resulting afterglow intensity is stronger than under near UV excitation. At 382 nm, Eu^{2+} ions on both Sr^{2+} sites in $SrAl_2O_4$ are excited, but at room temperature the blue emission is quenched, leading to a loss of photons. The observed effects can further be associated with the ratio of Eu^{2+} ions and trap states which are modulated by the concentrations of Eu^{2+} and Dy^{3+} in $SrAl_2O_4$, as well as by temperature. Increasing the nominal Dy^{3+} content from 0.1 mol% to 0.5 mol% with respect to Sr results in the doubling of the integrated afterglow intensity and confirms thus that Dy^{3+} ions are indeed involved in the trapping process. The concentration of trap states is much lower than the concentration of Eu^{2+} ions, as even with low excitation densities, a plateau of integrated afterglow intensity (corresponding to the total number of accessible traps) is reached. We postulate that an important fraction of excited Eu^{2+} ions can potentially transfer their energy to trap states. Once that all traps are filled or in a dynamical filling-depletion process under illumination (with thermal and/or optical depletion processes), for the remaining Eu^{2+} a "normal" steady-state emission is observed. The luminescence decay curves at 520 nm measured at 77 K show a mono-exponential decay with a common lifetime of about 1140 ns for all 5 samples under 437 nm excitation, while under 375 nm excitation, a feed process originating from the energy transfer between Eu^{2+} ions is demonstrated. Under 375 nm excitation, the non-exponential decay observed at 440 nm can be quantitatively associated to a Förster energy transfer process with $R_0 = 1.58$ (8) nm. For the overall understanding of the afterglow processes, it appears that one has to consider the individual contributions of all active ions on different lattice sites.
© 2021 The Authors. Published by Elsevier B.V. on behalf of Chinese Society of Rare Earths. This is an open access article under the CC BY-NC-ND license (http://creativecommons.org/licenses/by-nc-nd/4.0/).

1. Introduction

Long persistent phosphors attract an increasing interest.[1–5] To date, $SrAl_2O_4:Eu^{2+},Dy^{3+}$ is the best performing non-radioactive persistent phosphor material, and many papers have addressed various aspects related to the proposed mechanisms of trapping and detrapping in this material.[1–4] Afterglow can be observed in europium-only doped $SrAl_2O_4$, but the addition of Dy^{3+} has been

☆ **Foundation item:** Project supported by the Swiss National Science Foundation (200020_182494, 200021_169033) and Innosuisse (25902.1 PFNM-NM, 15217.1 PFIW-IW).
* Corresponding author.
E-mail address: hans-rudolf.hagemann@unige.ch (H. Hagemann).

https://doi.org/10.1016/j.jre.2021.07.014
1002-0721/© 2021 The Authors. Published by Elsevier B.V. on behalf of Chinese Society of Rare Earths. This is an open access article under the CC BY-NC-ND license (http://creativecommons.org/licenses/by-nc-nd/4.0/).

shown to dramatically improve the performance of this persistent phosphor.[1–4] In $SrAl_2O_4$, it appears that the ground state energy level of Dy^{2+} is optimally located below the conduction band to accept an electron from the excited d states of Eu^{2+}, generating thus an electron trap corresponding to a Eu^{3+}-Dy^{2+} species.[6,7] Co-doping with other rare earth ions leads to lower afterglow intensities.[8]

Europium ions can occupy the two different Sr lattice sites in $SrAl_2O_4$.[9] This fact has not frequently been addressed explicitly in studying the afterglow properties of this persistent phosphor. The recent reviews on this materials[3,4] do not explicitly address the effects due to the presence of two different europium ions on the energy transfers involved in the afterglow processes. At low temperature, two emission bands are observed at *ca.* 440 (blue) and 515 nm (green), which are assigned to the Eu^{2+} ions on the two different Sr sites.[10–13] The blue emission at 440 nm is quenched at room temperature.

We have shown previously that energy transfer takes place between blue and green emitting europium ions in $SrAl_2O_4$:Eu^{2+}.[11] Energy transfer between Eu^{2+} ions has also been reported for $Sr_4Al_{14}O_{25}$.[16] Botterman et al.[10] have shown that for $SrAl_2O_4$:Eu^{2+},Dy^{3+} with 435 nm excitation, trap filling is a thermally activated process and that the distribution of traps depends on the excitation wavelength. This observation was also confirmed by the study of thermoluminescence as a function of temperature and excitation wavelength reported in the literature.[14]

Fig. 1 illustrates schematically the different processes which are involved in the trap filling in the persistent phosphors. The downwards pointing arrow **1** corresponds to the 515 nm emission of $SrAl_2O_4$:Eu^{2+},Dy^{3+}, which corresponds also to the persistent emission. This implies that all traps involved in the persistent emission must transfer their energy back to the green emitting 5d level of Eu^{2+}. The upward pointing green and blue arrows **2** excite either exclusively the green emitting europium ion ($\lambda > 405$ nm), or both different Eu^{2+} ions. The undulating arrow **3** indicates non-radiative decay, as the blue emitting Eu^{2+} ion is quenched at room temperature.[10]

The energy levels associated to the blue emitting Eu^{2+} ions are shown in blue, those to the green emitting Eu^{2+} ion in green. To each different Eu^{2+} ion, a set of accessible trap states is associated with the same color (numbered **4** and **5**). The different TL curves measured with 445 and 375 nm excitation[14] show that more shallow traps, as illustrated by the convoluted TL peak at 300 K, are accessed with the excitation of the blue emitting Eu^{2+} ion. The trap states **4** and **5** assemble generically all possible traps which can be present: intrinsic defects,[15,16] boron related traps and rare earth related traps.[1–8] Different types of traps can thus be specifically addressed using differently doped samples.

Once the green emitting Eu^{2+} ion is excited, it can either emit (green downwards pointing arrow) or fill the traps either directly (thermally assisted[10] and/or tunneling) or via the conduction band (dashed arrows).[17] These processes are generically labelled **6** in Fig. 1 and apply also to the trap filling processes from the excited state of the blue emitting Eu^{2+} ion. The depletion of the traps can take place either from thermal excitation (not shown in the figure), or by optically stimulated luminescence (OSL), labelled **8**.[10,18,19] With 382 nm excitation, also the blue emitting europium ion is excited, adding the processes **10** on the left hand side of Fig. 1. Ueda

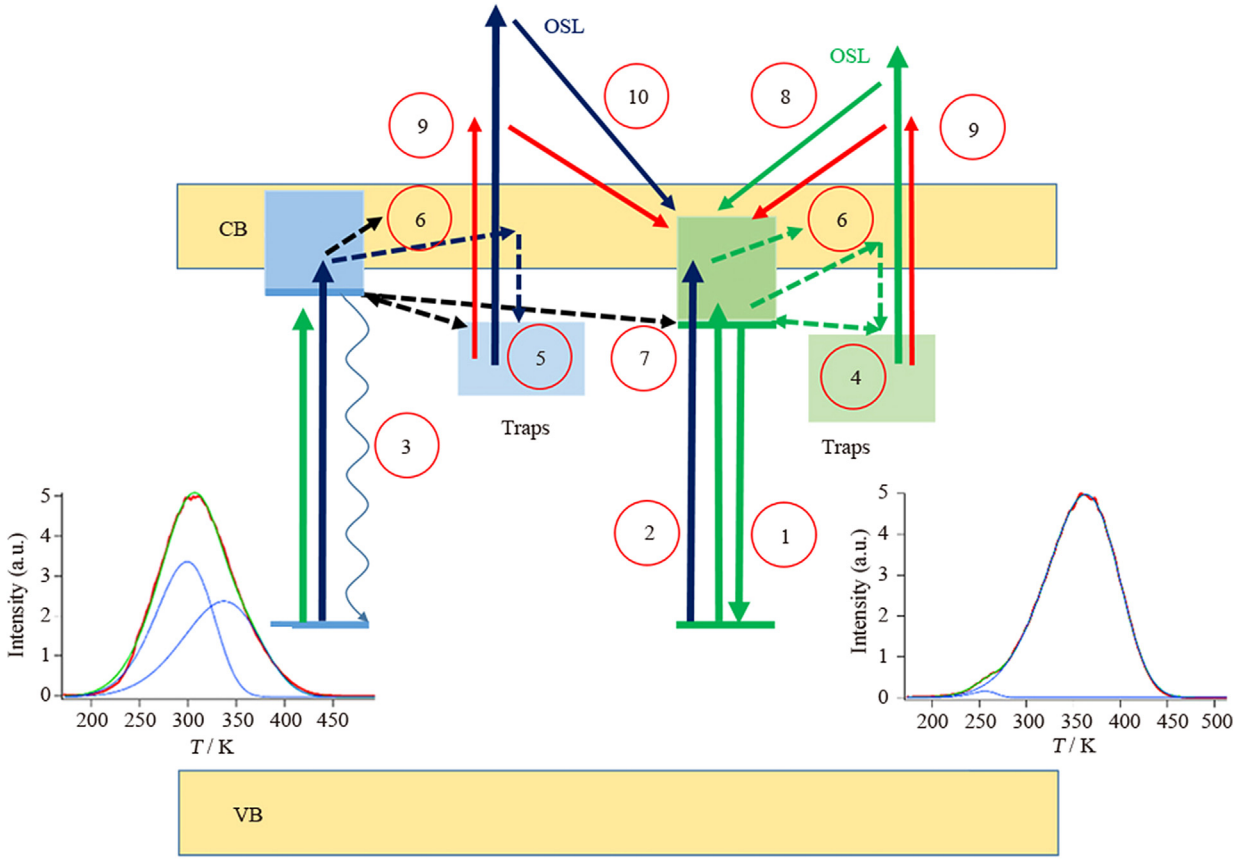

Fig. 1. Schematic illustration of trap filling and depletion processes in $SrAl_2O_4$:Eu^{2+},Dy^{3+} discussed in the text. The insets show the thermoluminescence (TL) curves after blue (right side) and near UV (left side) excitation at −100 °C.[14]

et al.[17] reported the observation of photoconductivity at room temperature under blue and near UV excitation, this is indicated by the arrows pointing directly into the conduction band. This process is also included in **6,** as the transfer to the conduction band can then lead either to trap filling or energy dissipation. Finally, process **9** corresponds to the trap depletion under NIR irradiation, which has been reported by several authors.[20,21]

In this work, we recall the possible transfer processes related to the afterglow in the persistent phosphors $SrAl_2O_4$:Eu^{2+},Dy^{3+} and $Sr_4Al_{14}O_{25}$:Eu^{2+},Dy^{3+} into a simplified diagram which addresses explicitly both different Eu^{2+} ions in these lattices. We then probe experimentally the effect of dopant concentration, illumination intensity and temperature on the afterglow behavior of different Eu^{2+} and Dy^{3+}-doped $SrAl_2O_4$ samples under blue excitation (444 nm) and under near UV excitation (382 nm) which excites the Eu^{2+} ions on both lattice sites, probing thus either selectively only the right hand side of Fig. 1 or the entire scheme. Additionally, the energy transfer between the two different europium ions is quantitatively analyzed.

2. Experimental

2.1. Samples preparation

Samples (see Table 1) were prepared as reported previously[11,14,22,23] by a solid-state reaction. Stoichiometric amounts of $SrCO_3$ and Al_2O_3 together with Eu_2O_3 and Dy_2O_3 were thoroughly mixed using a ball mill. Small portion of boric acid was added as flux to improve the crystallization[24] and afterglow performance.[14] The ratio Al/(Sr + Eu) was fixed exactly to 2/1. The mixtures were then annealed for 4 h under reducing conditions at 1450 °C (5% H_2 in argon) in a tube furnace. The resulting particle size does not depend on the rare earth doping. Our synthesis procedure is fully reproducible and has been repeated for several hundreds of samples[25] to yield always high purity samples with more than 95% of the title compound, as shown by our previously published X-ray analyses[11,14,23] and the X-ray diffraction data for samples 1–5 in Fig. 2. For comparison reasons (afterglow pigments should show a similar grain-size distribution) all sintered samples have been milled in a mortar and sieved to reach final d_{50} and d_{90} values of approximately 25 and 45 μm, respectively without any further treatment or purification.

2.2. Loading and afterglow experiments

In a pre-experiment, the maximum amount of pigment is evaluated (15 mg/cm^2 on a white pre-coated aluminum plate) to have a linear increase of luminous intensity relative to the quantity of pigment applied. Once a non-linearity starts we get self-absorption effects. All measurements have been done with 15 mg/cm^2 samples. This concentration has thus been shown to be optimal (enough sample for good signal, not too much to avoid that not all of the powder is equally exposed to the light source). Note that this concentration of 15 mg/cm^2 is well in the linear range for quantitative afterglow experiments reported by Van der Heggen et al.[26] The temperature of the sample is controlled by a Peltier element.

Table 1
Nominal dopant concentrations relative to strontium ($Sr_{1-x-y}Al_2O_4$:Eu_x,Dy_y).

Samples	Eu conc. (rel. to Sr)	Dy conc. (rel. to Sr)
1	0.0105	0.0025
2	0.015	0.0025
3	0.0075	0.0025
4	0.0105	0.005
5	0.0105	0.001

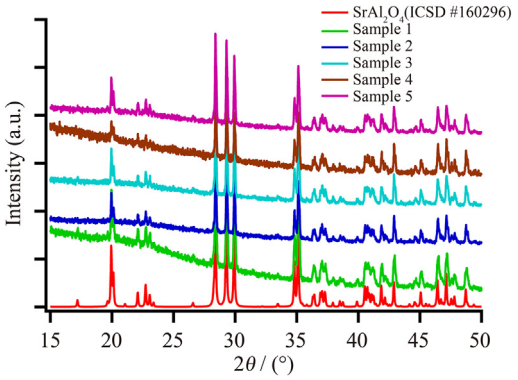

Fig. 2. Room temperature powder X-ray (Cu Kα) diffraction data for samples 1–5, together with the reference data for $SrAl_2O_4$.

Brightness (afterglow intensity) and maximum luminescence were measured with a LMT (Lichtmesstechnik Berlin) 1100 Photometer. Dependent on the excitation power, the charging time was varied between 30 min (low excitation power) and 10 min (high excitation power) to reach the equilibrium between trapping and de-trapping, corresponding to a steady state emission. Once the steady state is reached, additional loading time has no effect on the afterglow curve, as all accessible traps have been filled. Examples of loading curves can be seen in various papers.[18,24]

The variation of the excitation power was adjusted by a classical dimmer. Emission and excitation spectra were measured with a Varian Cary Eclipse fluorescence spectrometer. Intensity of the blue LED was measured with a Konica Minolta CL-70F luxmeter. Excitation power and number of photons were calculated in accordance to the emission spectra. Excitation power of the UV LED was measured with a Hönle UV meter equipped with an UV A measuring head. The number of photons was calculated in accordance to the emission spectra.

2.3. Time resolved emission experiments

Two pulsed laser-diodes were used as excitation light sources (437 nm, PicoQuant LD-440; 375 nm, PicoQuant LD-375 with a 360 nm bandpass filter) with *ca.* 5–10 pJ on a spot with a diameter (using the 1/e definition) of approx. 30 μm resulting in a fluence of *ca.* 1 μJ/cm^2. The repetition rate of the light source was 62.5 – 250 kHz (depending on the time-range of the observed emission decay). The polarization of the excitation was controlled using a Glan-Taylor polarizer and set to s-polarization. Fluorescence of the samples at 77 K was collected using a Cassegrain type collection optic (Anagrain; Anaspec Research Laboratories Ltd., Berkshire, UK) in 180° back-scattering geometry, passed through appropriate long-pass filters (409 or 458 nm), a wire-grid polarizer (Thorlabs, WP25M–UB) at magic angle with respect to the excitation, and focused onto a fiber using an achromatic lens (Thorlabs, AC254-100-AB). A Triax-190 (Horiba) imaging spectrograph with a 150 lines/mm grating (λ_{blaze} = 500 nm) was used to disperse the fluorescence coming from the multimode fiber (= 200 μm, NA 0.012, CeramOptec). For all samples detection wavelengths of 440 and 530 nm and a bandpass of approx. 2 nm were used. The spectrally dispersed light exiting the spectrograph was focused on a single-photon avalanche diode (Micro Photon Devices, MPD-100-CTE) with the help of an elliptic mirror (Horiba, 1427C). The time-correlated single photon counting was performed with a PicoHarp-300 (PicoQuant). The raw time-resolved data were

binned into a linear-logarithmic time-grid, with times smaller than 40 times the raw step-size (0.064–0.512 ns) maintaining the linear grid, and with times larger being binned into a logarithmic grid with 40–60 bins per decade. The statistical (Poisson) noise was calculated accordingly. The goodness of fit was judged by the reduced χ_r^2 value, calculated according to Eq. (1):

$$\chi_r^2 = \frac{1}{N-1-p}\sum_{i=1}^{N}\left(\frac{I_i - F_i}{\sigma_i}\right)^2 \quad (1)$$

where N is the total number of (re-binned) experimental points, p is the number of fitting parameters, I_i are the experimental data, F_i is the fit value at position i, and σ_i is the experimental standard deviation at point i.

3. Results and discussion

3.1. Excitation spectrum and LED emissions

The room temperature excitation spectrum of the green emission is shown in Fig. 3. This emission spectrum remains unchanged upon co-doping with other rare earth ions instead of Dy^{3+}.[8] Detailed spectroscopic studies of $SrAl_2O_4$ co-doped with Eu^{2+} and Dy^{3+} show that the excitation spectrum shown in Fig. 3 corresponds to the dipole allowed f-d absorptions of the divalent Eu^{2+} ion.[10] The excitation bands of Dy^{3+} observed for a sample without Eu^{2+} are around 320, 348, 364, 386, 425 and 453 nm.[27] In Eu^{2+},Dy^{3+} codoped samples, the emission of Dy^{3+} is not observed, as it is masked by the much stronger Eu^{2+} emission and afterglow. Absorption spectra of a single crystal of $SrAl_2O_4$ co-doped with Eu^{2+} and Dy^{3+} showed in the NIR region absorption bands of Dy^{3+}, confirming that Dy^{3+} effectively enters the crystal lattice.[22]

Fig. 3 equally shows the emission spectra of the blue and near UV LED used for the afterglow studies. It can be seen that the blue excitation is at the low energy edge of the excitation spectrum of the 520 nm emission, and excites thus selectively only one of the 2 europium ions in the lattice.

3.2. Effect of excitation power on luminescence at equilibrium (charging/de-charging) and the amount of trapped charge carriers

Fig. 4 shows the effect of the excitation power on the maximum fluorescence intensity under blue and near UV excitation. This intensity reflects the steady state emission under constant illumination. With low intensity illumination (below 40×10^{15} photons/s), the increase is higher than linear under both illuminations, while with higher illumination intensities, the increase is linear. The maximum illumination power of our set-up is not sufficient to saturate the Eu^{2+} emission.

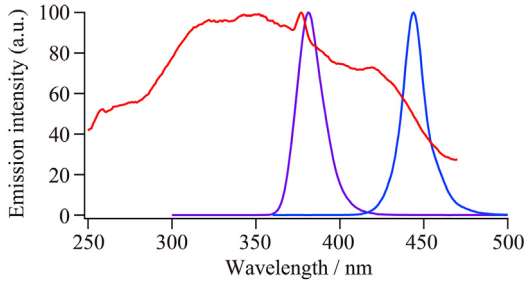

Fig. 3. Room temperature excitation spectrum of $SrAl_2O_4$:Eu^{2+},Dy^{3+} of the emission band at 515 nm (red trace) and the emission spectra of the two LED lamps used to excite the phosphors in this study (blue trace 444 nm LED, violet trace 382 nm LED).

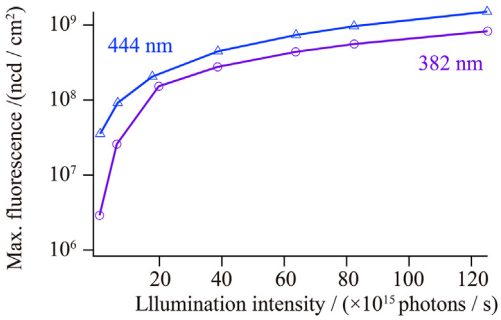

Fig. 4. Maximum steady state fluorescence intensity under 444 nm (blue trace) and 382 nm (violet trace) excitation at 25 °C as a function of illumination intensity.

Fig. 5 shows the integrated afterglow intensity from 0 to 10 min after switching off the LED. The ratio of the integrated afterglow intensity (0–10 min) to the integrated afterglow intensity (0–60 min) is constant within experimental error (+/−2%). Above *ca.* 10^{16} photons/s, this integrated intensity is more or less constant, even under the highest illumination of 1.25×10^{17} photons/s. This observation indicates that the total number of traps is small compared to the total number of Eu^{2+} ions, as all accessible traps are filled with an illumination power of about 10^{16} photons/s, which is orders of magnitude less than required to saturate the Eu^{2+} emission. Note that a slight decrease with increasing power is observed for both UV and blue illumination. The origin of this decrease is not clear. It could be either associated with a slight local heating during illumination (associated with some shallow trap depletion which are measured here in the first 10 min), or alternatively with an OSL mechanism during illumination,[18] or with some undefined experimental artefacts.

3.3. Effect of excitation wavelength on afterglow

Fig. 6 presents the afterglow intensity for sample 1 after blue and near UV excitation. All afterglow curves are non-linear on a log-log scale.

With the same number of exciting photons, the resulting afterglow brightness is about 1.5–2 times larger under blue vs near UV excitation. On the first glimpse this may appear surprising, as the extinction coefficient at 370 nm is much larger than that at 440 nm.[22] However, in the near UV, the blue emitting Eu ions are also excited, but their emission is quenched, indicating that photons are lost non-radiatively in the process,[10] while above 400 nm, only the green emitting Eu ion is excited (see also discussion below).

This experiment was repeated for dilute and more concentrated Eu-doped $SrAl_2O_4$ to probe the effect of energy transfer between Eu

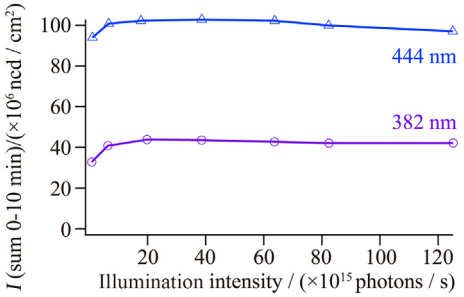

Fig. 5. Integrated afterglow intensity (0–10 min after illumination) under 444 nm (blue trace) and 382 nm (violet trace) excitation at 25 °C as a function of illumination intensity.

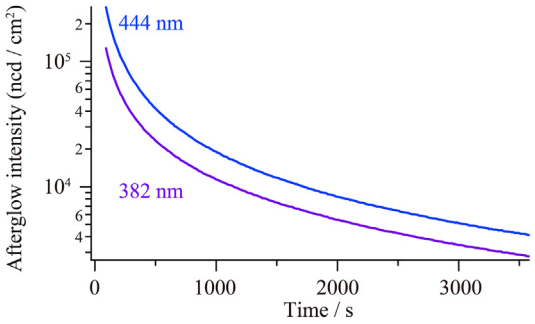

Fig. 6. Afterglow intensity for sample 1 at 25 °C after blue (blue line) and near UV (violet line) illumination with 4.65×10^{18} (blue) and 5.54×10^{18} (UV) photons in 2 min.

Table 2
Brightness at different times under blue excitation (444 nm) as a function of dopant concentration at 25 °C. The full data for sample 1 are shown in Fig. 4. The accuracy of the data is *ca.* 2%.

	Brightness (ncd/cm²)			Brightness (ncd/cm²)		
Samples	3	1	2	5	1	4
Eu (mol%)	0.7	1.05	1.5	1.05	1.05	1.05
Dy (mol%)	0.25	0.25	0.25	0.1	0.25	0.5
2 min	230829	203134	207000	150910	203134	265376
5 min	83438	74504	74688	55093	74504	96898
30 min	10456	9455	9480	7136	9455	11891
60 min	4471	4108	4041	3107	4108	5034

ions (see Tables 2 and 3). With increasing Eu concentration, the brightness of the afterglow under blue excitation decreases, while it increases upon near UV excitation. The presence of Dy^{3+} in the persistent phosphor $SrAl_2O_4$:Eu^{2+},Dy^{3+} improves dramatically the afterglow properties[1–4] which has been associated to "Eu^{3+}-Dy^{2+}" trap species.[6] Thus, increasing the nominal Dy-content is expected to increase the number of accessible traps and thus the afterglow performance. The experiments done here show that this is indeed the case, as a significantly increased brightness under both blue and near-UV excitation is observed with increasing nominal Dy^{3+} concentration.

3.4. Effect of temperature

The ratio of brightness resulting from blue excitation and near UV excitation at different temperatures is shown in Fig. 7. At lower temperatures and relatively short afterglow times, the initial brightness is much higher under blue excitation, while for longer afterglow time (>45 min), this ratio is more or less constant. This

Table 3
Brightness at different time under near UV excitation (382 nm) as a function of dopant concentration at 25 °C. The full data for sample 1 are shown in Fig. 5. The accuracy of the data is *ca.* 2%.

	Brightness (ncd/cm²)			Brightness (ncd/cm²)		
Samples	3	1	2	5	1	4
Eu (mol%)	0.7	1.05	1.5	1.05	1.05	1.05
Dy (mol%)	0.25	0.25	0.25	0.1	0.25	0.5
2 min	92368	98145	115858	72289	98145	133981
5 min	36253	38881	45616	29446	38881	51135
30 min	5559	6139	6890	4813	6139	7415
60 min	2519	2798	3090	2202	2798	3274

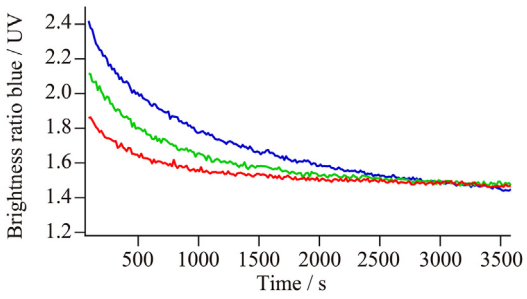

Fig. 7. Relative brightness (blue excitation/UV excitation) observed at 5 °C (blue trace), 25 °C (green trace) and 45 °C (red trace) for sample 1.

observation suggests that under blue illumination, more shallow traps are populated than under UV excitation. With increasing temperature, shallow traps are also thermally depleted (in part during illumination), and this results in the observed reduction of relative brightness for short (<10 min) afterglow times. This is also in line with the experiments reported by Botterman et al.[10] for $SrAl_2O_4$:Eu, Dy under 370 and 435 nm excitation. Under blue illumination, the integrated afterglow and TL emission decrease much more under blue excitation than under UV excitation when the temperature is increased from 280 to 320 K (see Figs. 6 and 7 in Ref. 10.)

3.5. Decay curves measured at 77 K

Upon excitation at 437 nm, the emission band at 520 nm shows a mono-exponential decay with a lifetime of $\tau_{520\ nm} = 1120\ (20)$ ns for all 5 samples. Illumination at 375 nm excites both Eu^{2+} ions. The decay of the emission at 440 nm proceeds non-exponentially and is best reproduced using the Inokuti-Hirayama static quenching model via Förster resonance energy transfer Eq. (2)[28]:

$$F_{440\ nm}(t) \propto \exp\left(-\frac{t}{\tau_{440\ nm}} - \frac{4\pi^{3/2}}{3} c R_0^3 \sqrt{\frac{t}{\tau_{440\ nm}}} \right) \quad (2)$$

$\tau_{440\ nm}$ is the intrinsic (infinite dilution) emission lifetime of the donor Eu^{2+} emitting at 440 nm, c its concentration and R_0 the Förster radius. This model reproduces the experimental data requiring a donor lifetime of 900 (100) ns and a Förster radius of $R_0 = 1.58\ (8)$ nm. Fig. 8 compares the data obtained for samples 2 and 3 to illustrate the observed and fitted curves and highlight the effect of Eu^{2+} concentration.

The emission decay curves observed at 520 nm under 375 nm excitation show first a rise caused by the energy transfer from the blue emitting to the green emitting Eu ion and then the decay. The experimental data can be described by Eq. (3):

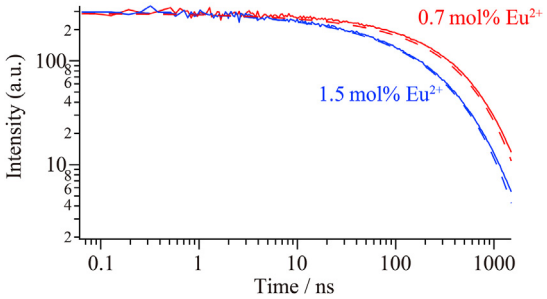

Fig. 8. Observed (full line) and fitted (dashed line) decay curves of the emission at 440 nm under 375 nm excitation at 77 K. Blue traces: Sample 2; Red traces: Sample 3.

$$F_{520\ \mathrm{nm}}(t) \propto e^{-\frac{t}{\tau_{520\ \mathrm{nm}}}} - XF_{440\ \mathrm{nm}} \quad (3)$$

When the decay of the donor is significantly faster than the decay of the acceptor, the parameter X can be related to the ratio of the extinction coefficients of donor and acceptor at the excitation wavelength of 375 nm via Eq. (4):

$$\frac{\varepsilon_{440\ \mathrm{nm}}(375\ \mathrm{nm})}{\varepsilon_{520\ \mathrm{nm}}(375\ \mathrm{nm})} = \frac{X}{1-X} \quad (4)$$

Using the result for $F_{440\ \mathrm{nm}}(t)$ obtained from the first fit as input and the ratio of the extinction coefficients and the acceptor lifetime $\tau_{520\ \mathrm{nm}}$ as adjustable parameters, the data are excellently reproduced. The values of $\tau_{520\ \mathrm{nm}}$ obtained from this fit agree within experimental error with those obtained separately from the decay curves under blue excitation. The ratio of extinction coefficients is found to be 0.6 ± 0.2. The reduced χ_r^2 value is close to 1 in all cases.

3.6. Discussion of the combined results

The observations shown above can be qualitatively explained as follows. Bierwagen et al.[14] demonstrated by TL measurements the creation of different shallow and deep traps by boron and/or Dy addition. Very recently, it has been shown that there are very deep traps (with a maximum at *ca.* 300 °C in the TL curves) as well as shallow traps in $SrAl_2O_4$:Eu^{2+},Dy^{3+}.[29] We claim similarly as in previous report[29] that each Eu atom is connected to a trap, but the number of traps is significantly smaller than the amount of Eu atoms,[26] which means that some Eu atoms are connected to the same trap. Note that these traps may be shallow or deep. During charging we can see now following effects: In the very beginning of the charging process we see "no" luminescence, as all excited electrons will be trapped (as all Eu atoms are connected to a trap and the trapping process (some kind of electron transfer) is much faster than the lifetime of the excited 5 d^1 state of Eu^{2+}). This corresponds also to the observation and analysis of the loading curve reported in the literature.[18] Afterwards we see the typical increase of luminescence until we reach the equilibrium between charging and de-charging.[18] This increasing loading curve results from the increased de-charging of trapped charge carriers and of an increasing amount of directly fluorescent Eu atoms (Eu atoms, which cannot trap, as the trap is already trapped by another Eu atom). With increasing intensity the charging of the traps turns faster, but also the amount of "only fluorescent Eu atoms" increases. Once all traps are charged, a further increase of the excitation power leads to the observed linear increase of luminescence (Fig. 4), as in our experiments the power remains too low to saturate this "normal" Eu^{2+} emission. In this power range, the plateau of maximum afterglow is observed (Fig. 4). Furthermore, as shown by the lifetime measurements above, there is an energy transfer from the blue emitting Eu^{2+} to the green emitting Eu^{2+} and at room temperature, the emission of the blue emitting Eu^{2+} ion is quenched.[10] The detailed nature of the charging process is not clear at present. As shown in Fig. 1, both local energy transfers, and processes through the conduction band can take place. Processes through the conduction band are more likely to occur under near UV illumination, as Ueda et al.[17] have reported the observation of low temperature photoconductivity in $SrAl_2O_4$ upon irradiation at 400 nm and shorter wavelengths. At room temperature also irradiation at 440 nm yields a measurable photocurrent.[17] Although a photocurrent is observed under UV or 400 nm excitation, it is not clear, whether these processes are real trapping or processes like radiationless quenching via the conduction band.

In the first experiment (see Fig. 5 above), under blue excitation, all the green emitting Eu^{2+} ions absorb the light and lead to a strong afterglow intensity (brightness), which indicates a rather efficient charging of the traps. Under near UV excitation both blue and green emitting Eu^{2+} ions are excited, but the blue emitting Eu^{2+} is quenched at ambient temperature. Another contribution to the lower afterglow intensity under near UV excitation can be the optically stimulated emission during the charging process reported by Smet et al.,[18] which contributes to a partial depletion of the trapped states. Even with increased UV excitation intensity, the afterglow intensities remain smaller than the one achieved under blue excitation.

Increasing the Eu^{2+} concentration has a priori two effects. As the number of trap states is typically related to local defects, this number should not be affected significantly by the additional isovalent substitution of Sr^{2+} ions by Eu^{2+} ions which both have similar ionic radii. This means that the ratio between Eu^{2+} ions and accessible trap states is shifted (there are more Eu^{2+} ions). Further, with increasing Eu^{2+} concentration, the energy transfer between Eu^{2+} ions becomes more efficient (see Fig. 8). Under blue excitation, the brightness of the afterglow decreases, which can be explained by the fact that a larger fraction of photons are absorbed and directly reemitted by the isolated Eu^{2+} ions, as a smaller fraction of photons contribute to the charging process. Under near UV excitation, the brightness increases, which suggests that the energy transfer from blue to green emitting Eu^{2+} ions contributed to this increase.

It has been established[1–4] that the afterglow intensity increases strongly with the co-doping with Dy^{3+}. Increasing the Dy^{3+} content leads to an increased number of trap states. This implies that the ratio between Eu^{2+} ions and trap states is now shifted towards the trap states (at constant Eu^{2+} content), i.e., there are more traps available. Under both blue and near UV excitation, the brightness increases strongly, as there are many more traps which can be reached with the same excitation (and a smaller fraction of Eu^{2+} ions directly re-emits the absorbed photons).

4. Conclusions

We have constructed a general scheme to address systematically the processes associated to the persistent emissions in strontium aluminates, distinguishing explicitly the two different Eu^{2+} ions in the crystal structures of $SrAl_2O_4$:Eu^{2+},Dy^{3+} and $Sr_4Al_{14}O_{25}$:Eu^{2+},Dy^{3+}.[30] The experiments reported here show that indeed the excitation wavelength has a significant impact on the afterglow of $SrAl_2O_4$ doped with Eu^{2+}. Under blue excitation, more shallow traps are filled, as shown by the temperature dependent experiments. The observed differences between blue and near UV excitation can be associated to the thermal quenching of the blue emitting Eu^{2+} ions, to the energy transfer between Eu^{2+} ions, to the number of available traps (modulated here by the concentration of Dy^{3+} ions), and probably also to the OSL which appears to be more efficient in the near UV. With different relative Eu^{2+} and Dy^{3+} doping, it is possible to modulate the ratio of Eu^{2+} ions and traps, which impacts on the resulting afterglow. Further investigations are under way and will be published shortly.

References

1. Matsuzawa T, Aoki Y, Takeuchi N, Murayama Y. A new long phosphorescent phosphor with high brightness, $SrAl_2O_4$:Eu^{2+},Dy^{3+}. *J Electrochem Soc.* 1996;143:2670.
2. Van den Eeckhout K, Smet PF, Poelman D. Persistent luminescence in Eu^{2+}-doped compounds: a review. *Materials.* 2010;3:2536.

3. Rojas-Hernandez RE, Rubio-Marcos F. Rodriguez MÁ, Fernandez JF. Long lasting phosphors: $SrAl_2O_4$:Eu,Dy as the most studied material. *Renew Sustain Energy Rev*. 2018;81:2759.
4. Vitola V, Millers D, Bite I, Smits K, Spustaka A. Recent progress in understanding the persistent luminescence in $SrAl_2O_4$:Eu,Dy. *Mater Sci Technol*. 2019;35:1661.
5. Sun WZ, Tan T, Cai JZ, Zhang HW. Bright yellow-emitting long persistent luminescence from Mn^{2+}-activated strontium aluminate phosphor. *J Rare Earths*. 2021. https://doi.org/10.1016/j.jre.2021.05.006.
6. Dobrowolska A, Cihan Karsu E, Bos AJJ, Dorenbos P. Spectroscopy, thermoluminescence and afterglow studies of $CaLa_4(SiO_4)_3O$: Ln (Ln= Ce, Nd, Eu, Tb, Dy). *J Lumin*. 2015;160:321.
7. Joos JJ, Korthout K, Amidani L, Glatzel P, Poelman D, Smet PF. Identification of Dy^{3+}/Dy^{2+} as electron trap in persistent phosphors. *Phys Rev Lett*. 2020:125, 033001.
8. Katsumata T, Toyomane S, Sakai R, Komuro S, Morikawa T. Trap levels in Eu-doped $SrAl_2O_4$ phosphor crystals Co-doped with rare-earth elements. *J Am Ceram Soc*. 2006;89:932.
9. Schulze AR, Buschbaum HM. Compound formation $MeO:M_2O_3$. IV. Structure of Monoclinic $SrAl_2O_4$. *Z Anorg Allg Chem*. 1981;475:205.
10. Botterman J, Joos JJ, Smet PF. Trapping and detrapping in $SrAl_2O_4$:Eu,Dy persistent phosphors: influence of excitation wavelength and temperature. *Phys Rev B Condens Matter*. 2014;90, 085147.
11. Bierwagen J, Yoon S, Gartmann N, Walfort B, Hagemann H. Thermal and concentration dependent energy transfer of Eu^{2+} in $SrAl_2O_4$. *Opt Mater Express*. 2016;6:793.
12. Nazarov M, Brik MG, Spassky D, Tsukerblat B. Crystal field splitting of 5d states and luminescence mechanism in $SrAl_2O_4$:Eu^{2+} phosphor. *J Lumin*. 2017;182:79.
13. Ning L, Huang X, Huang Y, Tanner PA. Origin of the green persistent luminescence of Eu-doped $SrAl_2O_4$ from a multiconfigurational *ab initio* study of $4f^7 \rightarrow 4f^6 5d^1$ transitions. *J Mater Chem C*. 2018;6:6637.
14. Bierwagen J, Delgado T, Jiranek G, Yoon S, Gartmann N, Walfort B, et al. Probing traps in the persistent phosphor $SrAl_2O_4$:Eu^{2+},Dy^{3+},B^{3+} - a wavelength, temperature and sample dependent thermoluminescence investigation. *J Lumin*. 2020;222, 117113.
15. Finley E, Mansouri Tehrani A, Brgoch J. Intrinsic defects drive persistent luminescence in monoclinic $SrAl_2O_4$:Eu^{2+}. *J Phys Chem C*. 2018;122, 16309.
16. Vitola V, Millers D, Smits K, Bite I, Zolotarjovs A. The search for defects in undoped $SrAl_2O_4$ material. *Opt Mater*. 2019;87:48.
17. Ueda J, Nakanishi T, Katayama Y, Tanabe S. Optical and optoelectronic analysis of persistent luminescence in Eu^{2+}-Dy^{3+} codoped $SrAl_2O_4$ ceramic phosphor". *Phys Status Solidi (c)*. 2012;9:2322.
18. Van der Heggen D, Joos JJ, Smet PF. Importance of evaluating the intensity dependency of the quantum efficiency: impact on LEDs and persistent phosphors. *ACS Photonics*. 2018;5:4529.
19. Tydtgat C, Meert KW, Poelman D, Smet PF. Optically stimulated detrapping during charging of persistent phosphors. *Opt Mater Express*. 2016;6:844.
20. Chithambo ML. Thermal assistance in the optically stimulated luminescence of superluminous $Sr_4Al_{14}O_{25}$: Eu^{2+},Dy^{3+}. *Phys B*. 2021;603, 412722.
21. Liu H, Feng B, Luo L, Han C, Tanner PA. Near infrared photostimulated persistent luminescence and information storage of $SrAl_2O_4$:Eu^{2+},Dy^{3+} phosphor. *Opt Mater Express*. 2016;6:3375.
22. Delgado T, Afshani J, Hagemann H. Spectroscopic study of a single crystal of $SrAl_2O_4$:Eu^{2+}:Dy^{3+}. *J Phys Chem C*. 2019;123:8607.
23. Hagemann H, Lovy D, Yoon S, Pokrant S, Gartmann N, ierwagen J, et al. Wavelength dependent loading of traps in the persistent phosphor $SrAl_2O_4$:Eu^{2+}, Dy^{3+}. *J Lumin*. 2016;170:299.
24. Chang YL, Hsiang HI, Liang MT. Characterizations of Eu,Dy co-doped $SrAl_2O_4$ phosphors prepared by the solid state reaction with B_2O_3 addition. *J Alloys Compd*. 2008;461:598.
25. Walfort B, Gartmann N, Yoon S, Pokrant S, Bierwagen J, Hagemann H. *Luminescent materials based on strontium aluminate and their preparation and use*. Patent WO 2016169700, 2016.
26. Van der Heggen D, Joos JJ. Rodríguez Burbano DC, Capobianco JA, Smet PF. Counting the photons: Determining the absolute storage Capacity of persistent phosphors. *Materials*. 2017;10:867.
27. Delgado T, Ajoubipour S, Afshani J, Yoon S, Walfort B, Hagemann H. Spectroscopic properties of Dy^{3+}- and Dy^{3+}, B^{3+}- doped $SrAl_2O_4$. *Opt Mater*. 2019;89:268.
28. Inokuti M, Hirayama F. Influence of energy transfer by the exchange mechanism on donor luminescence. *J Chem Phys*. 1965;43:1978.
29. Van der Heggen D, Vandenberghe D, Moayed NK, De Grave J, Smet PF, Joos JJ. The almost hidden role of deep traps when measuring afterglow and thermoluminescence of persistent phosphors. *J Lumin*. 2020;226, 117496.
30. Lin Y, Tang Z, Zhang Z, Nan CW. Anomalous luminescence in $Sr_4Al_{14}O_{25}$:Eu, Dy phosphors. *Appl Phys Lett*. 2002;81:996.